



# Dynamic Analysis of Functionally Graded Porous Beams Using Complementary Functions Method in the Laplace Domain

Ahmad Reshad Noori<sup>a</sup>, Timuçin Alp Aslan<sup>b</sup>, Beytullah Temel<sup>b</sup>

<sup>a</sup> Istanbul Gelişim University, Department of Civil Engineering, Istanbul, Turkey

<sup>b</sup> Çukurova University, Department of Civil Engineering, Adana, Turkey

## ARTICLE INFO

### Keywords:

Free vibration  
Forced vibration  
Functionally graded porous beam  
Viscoelastic materials  
Complementary Functions Method

## ABSTRACT

In this study, an efficient numerical procedure is introduced to the solution of the dynamic response of functionally graded porous (FGP) beams. The elastic modulus and mass density of the porous materials are considered to have non-uniform distributions along the thickness direction. The typical open-cell metal foam is assumed to govern the material constitutive law. Within the framework of the first-order shear deformation theory (FSDT) the influence of shear strain is included in the formulations. The impact of damping is also considered. By using the canonically conjugate momentums and their derivatives, the governing canonical equations of motion of FGP beams are derived for the first time. These equations are then transformed into the Laplace space and solved numerically with the aid of the Complementary Functions Method (CFM). Obtained results are retransformed to the time domain by using an efficient inverse transform method. The dynamic response of FGP beams is studied for several boundary and loading conditions. The suggested procedure is verified with the available published literature and the finite element method. Detailed parametric studies are conducted to show the influence of porosity constants, symmetric and asymmetric porosity distributions and damping ratios on the dynamic response of FG porous beams.

## 1. Introduction

New building materials are investigated by many researchers and scientists during the last decades because of the high demand for usage of these materials in the manufacturing of innovative engineering structures. Among these new building materials, FGP materials have become one of the main research focus across several engineering fields such as aerospace, automotive and civil engineering [1,2]. As one of the widely used FGPMs, metal foams have superb characteristics such as energy dissipation, thermal management, and stiffness to weight ratio, designable vibrational frequency as well as mechanical damping and electrical conductivity [3–6]. Sandwich plates, floor wall foam, sandwich panels, parking floor slab, balcony platforms, crane lifting arm, and support and race car crash absorbers, etc. can be shown as the usage of FGPMs in engineering applications [6]. These important characteristics and the wide range of usage of FGMs and FGPMs have attracted the attention of numerous researchers [7–24].

Biot [25] has discussed the buckling of a fluid-saturated porous slab. The elastic buckling response of the porous beams with a rectangular cross-section was investigated by Magnucki and Stasiewicz [26]. Chen et al. [27] applied the Ritz method to investigate the elastic

buckling and bending response of FGP beams based on the FSDT. Jamshidi et al. [28] suggested an optimization procedure for the post-buckling of two-dimensional FGP beams. The influence of porosity on static and dynamic behaviors of the FG beam was presented by Fouda et al. [29] based on the Euler-Bernoulli beam theory. The static analysis of 2D-FGP structures was investigated by Ramteke et al. [30] via the finite element method.

The differential transform method was used by Ebrahimi and Mokhtari [31] to carry out the natural frequencies of rotating FGP beams. Nonlinear vibration characteristics of FGP beams were obtained by Ebrahimi and Zia [32] with the help of the Galerkin and multiple scales methods. The natural frequencies of FGP beams were derived by Rjoub and Hamad [33] via a simple transfer matrix method. Chen et al. [34] examined the dynamic response of FGP beams by using step by step time integration method. Chen et al. [35] studied the nonlinear free vibration response of sandwich beams with FGP core. The dynamic analysis of FGP structures was examined by Wu et al. [36] with the aid of the finite element method. Akbaş [37] used the plane solid continua model to carry out the transient response of FGP deep beams. The vibration of deep curved and straight FGP beams was carried out by Zhao et al. [38]. A Jacobi-Ritz method

E-mail addresses: [arnoori@gelisim.edu.tr](mailto:arnoori@gelisim.edu.tr) (A.R. Noori), [taslan@cu.edu.tr](mailto:taslan@cu.edu.tr) (T.A. Aslan), [btemel@cu.edu.tr](mailto:btemel@cu.edu.tr) (B. Temel)

<https://doi.org/10.1016/j.compstruct.2020.113094>

Received 21 September 2020; Revised 2 October 2020; Accepted 4 October 2020

Available online 9 October 2020

0263-8223/© 2020 Elsevier Ltd. All rights reserved.

was applied by Qin et al. [39] to study the dynamic response of FGP beams. The unified approach of discrete singular convolution element method and Taylor series expansion method was used by Lei et al. [40] to investigate the vibration response of FGP beams.

The literature survey shows that most of the reported works are on the free vibration and undamped forced vibration of FGP beams while it is noticed that most of the aforementioned works do not consider the effect of damping. This study conducts the free, undamped, and damped forced vibration response of FGP beams. Both symmetric and asymmetric porosity distributions are considered. The classical beam theory (CBT) and FSDT have been adopted in the formulations. Also, in the damped forced vibration cases, the effect of damping of the FGP beams have been considered within the presented approach through the implementation of the Kelvin damping model. Closed-form solutions for the present class problem are not always available. For this reason, it is essential to develop efficient numerical approaches with a high level of accuracy and wide applicability. Moreover, this suggested scheme computes the unknown functions (for e.g., displacements) and their derivatives (for e.g., rotations) without any additional calculations. Also, it can be implemented for any distribution function of FGPMs. The CFM has been proven to be an accurate and efficient numerical approach previously [41–52].

The governing equations of motion are acquired by means of the minimum total energy principle. Then, by applying the canonically conjugate momentums and obtaining their derivatives, the governing canonical equations of free and forced responses of the FGP beams are derived for the first time. The derived canonical equations are transformed to the Laplace space and solved numerically for a set of Laplace series. To retransfer the results to the time domain, Durbin's modified Inverse Laplace transform is implemented. In the numerical solution of the canonical equations, a high order Runge–Kutta algorithm is applied. Consequently, an accurate unified analysis framework of the CFM and the Laplace transform is suggested in this study. The CFM will be attempted in the transferred domain to carry out the dynamic response in a simple and efficient manner, this method is infused into the analysis to convert the two-point value problems to a system of initial value problems. This system can be solved easily by any numerical method available in the literature, for example, the fifth-order Runge–Kutta method (RK5). The suggested method has excellent computational efficiency [41–52].

Free vibration and forced vibration responses of FGP Euler-Bernoulli's and Timoshenko's beams are obtained for various length to height ratios, several boundary conditions, such as clamped-clamped (C-C), Clamped-Free (C-F), and Clamped-Hinge (C-H). Both symmetric and asymmetric porosity distributions of FGPMs are considered. In the viscoelastic vibration response, the Kelvin type damping model is implemented. The influences of different parameters and porosity distributions on the vibration characteristics and transient response are examined and discussed in detail. So, the efficacious way to improve the vibration response of the FGP beams can be identified.

In order to present the paper in a better manner, it is organized as follows: Section 2 shows the derivation of canonically equations and the application of the suggested unified approach to the solution process. Subsequently, the efficiency and applicability of the proposed numerical method are demonstrated by several comparisons with the available literature and FEM. Several parametric studies are conducted in Section 3. Finally, the important conclusions of this research are given in Section 4.

## 2. Mathematical Formulations

### 2.1. Material models for FGPMs

A FGP beam is presumed with width  $b$ , thickness  $h$ , and length  $L$  as shown in Fig. 1. The x-axis of the coordinate system is in the longitu-

dinal direction while the z-axis is in the thickness direction. Within the scope of this research paper, it is presupposed that Young's modulus and mass density of the FGP beams are continuously changing in the thickness of the beam. The symmetric material constitutive relationships (SMCR) and monotonic material constitutive relationships (MMCR) are considered in this study (see [36]).

The functionally graded porosity for the SMCR model can be expressed by Eq. (1) for the MMCR model can be described by Eq. (2) (see [36]).

$$E(z) = E_1 \left[ 1 - \cos\left(\frac{\pi z}{h}\right) \right] + E_0 \cos\left(\frac{\pi z}{h}\right) = E_1 \left[ 1 - e_0 \cos\left(\frac{\pi z}{h}\right) \right]$$

$$G(z) = G_1 \left[ 1 - \cos\left(\frac{\pi z}{h}\right) \right] + G_0 \cos\left(\frac{\pi z}{h}\right) = G_1 \left[ 1 - e_0 \cos\left(\frac{\pi z}{h}\right) \right]$$

$$\rho(z) = \rho_1 \left[ 1 - \cos\left(\frac{\pi z}{h}\right) \right] + \rho_0 \cos\left(\frac{\pi z}{h}\right) = \rho_1 \left[ 1 - e_m \cos\left(\frac{\pi z}{h}\right) \right] \quad (1)$$

$$E(z) = E_1 \left[ 1 - \cos\left(\frac{\pi z}{2h} + \frac{\pi}{4}\right) \right] + E_0 \cos\left(\frac{\pi z}{2h} + \frac{\pi}{4}\right) = E_1 \left[ 1 - e_0 \cos\left(\frac{\pi z}{2h} + \frac{\pi}{4}\right) \right]$$

$$G(z) = G_1 \left[ 1 - \cos\left(\frac{\pi z}{2h} + \frac{\pi}{4}\right) \right] + G_0 \cos\left(\frac{\pi z}{2h} + \frac{\pi}{4}\right) = G_1 \left[ 1 - e_0 \cos\left(\frac{\pi z}{2h} + \frac{\pi}{4}\right) \right]$$

$$\rho(z) = \rho_1 \left[ 1 - \cos\left(\frac{\pi z}{2h} + \frac{\pi}{4}\right) \right] + \rho_0 \cos\left(\frac{\pi z}{2h} + \frac{\pi}{4}\right) = \rho_1 \left[ 1 - e_m \cos\left(\frac{\pi z}{2h} + \frac{\pi}{4}\right) \right] \quad (2)$$

In these equations,  $E_0$  and  $E_1$  are the minimum and maximum values of the modulus of elasticity,  $G_0$  and  $G_1$  are the minimum and maximum shear modulus values which can be obtained by the Eq. (3) (see [53]).

$$G_1 = \frac{E_1}{2(1 + \nu)}; G_0 = \frac{E_0}{2(1 + \nu)} \quad (3)$$

$\nu$  is the Poisson's ratio which is presumed to be constant [53].  $\rho_0$  and  $\rho_1$  are the minimum and maximum values of mass density. The porosity coefficient for the shear modulus and Young's modulus is given as (see [36]);

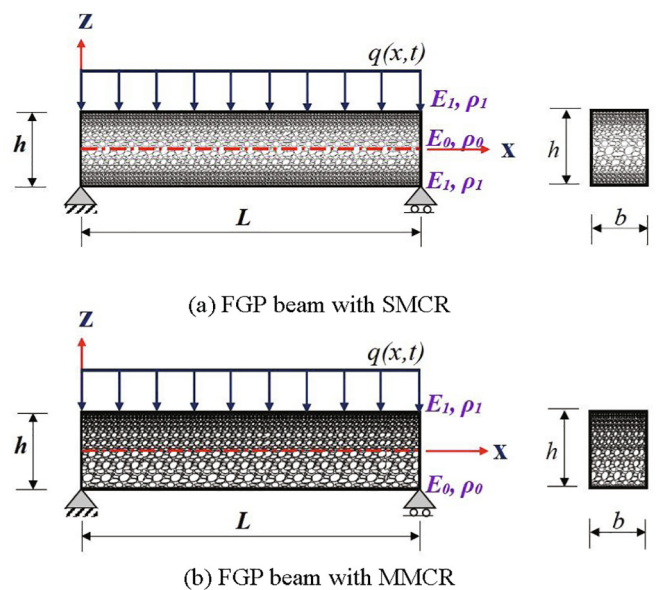


Fig. 1. Simply supported functionally graded porous beams with different porosity distributions.

$$e_0 = 1 - \frac{E_0}{E_1} \tag{4}$$

and the porosity coefficient for the mass density is (see [36]):

$$e_m = 1 - \frac{\rho_0}{\rho_1} \tag{5}$$

The relationship between the porosity coefficients can be expressed as [54]:

$$\frac{E_0}{E_1} = \left(\frac{\rho_0}{\rho_1}\right)^2 \rightarrow e_m = 1 - \sqrt{1 - e_0} \tag{6}$$

In the SMCR model, the mechanical properties of the material are symmetric about the mid-plane of the thickness. These quantities are maximum at the bottom and top surfaces of the cross-section and are minimum in the mid surface of the beam. In the MMCR model, the mechanical properties of the materials are asymmetric and they are decreasing from the top surface to the bottom surface. So, the maximum material properties are on the top surface while the minimum material properties are located at the bottom surface of the FGP beam.

2.2. Basic equations

The displacement field for the FGP beams based on the FSDT can be formulated as:

$$U_x = u(x, t) + z\theta(x, t) \tag{7}$$

$$U_z = w(x, t) \tag{8}$$

where  $t$  is time,  $U_x$  and  $U_z$  are the displacements in the axial direction and vertical deflection and  $\theta(x)$  is the rotation of mid-plane ( $z=0$ ). The strain field for the Timoshenko's beam can be given by:

$$\epsilon_x = \frac{\partial u}{\partial x} + z \frac{\partial \theta}{\partial x} \tag{9}$$

$$\gamma_{xz} = \theta + \frac{\partial w}{\partial x} \tag{10}$$

where  $\epsilon_x$  shows the normal strain and  $\gamma_{xz}$  denotes the shear strain. From the linear relations of stress and strain, the stress field of the FGP beams can be obtained as:

$$\sigma_x = E(z)\epsilon_x \tag{11}$$

$$\tau_{xz} = G(z)\gamma_{xz} \tag{12}$$

The total potential energy ( $\Pi_t$ ) of the FGP beam based on the FSDT can be given as:

$$\begin{aligned} \Pi_t &= \frac{1}{2} \int_0^L \int_A \left[ E(z) \left( \frac{\partial u}{\partial x} + z \frac{\partial \theta}{\partial x} \right)^2 + G(z) \left( \theta + \frac{\partial w}{\partial x} \right)^2 \right] dA dx - \int_0^L \int_A q w dA dx \\ &= \frac{1}{2} \int_0^L \int_A \left[ E(z) \left( \left( \frac{\partial u}{\partial x} \right)^2 + 2z \frac{\partial u}{\partial x} \frac{\partial \theta}{\partial x} + \left( z \frac{\partial \theta}{\partial x} \right)^2 \right) + G(z) \left( \theta^2 + 2\theta \frac{\partial w}{\partial x} + \left( \frac{\partial w}{\partial x} \right)^2 \right) \right] dA dx \\ &\quad - \int_0^L \int_A p_z w dA dx \\ &= \frac{1}{2} \int_0^L \left[ A_{11} \left( \frac{\partial u}{\partial x} \right)^2 + 2A_{12} \frac{\partial u}{\partial x} \frac{\partial \theta}{\partial x} + A_{22} \left( \frac{\partial \theta}{\partial x} \right)^2 + A_{33} \left( \theta^2 + 2\theta \frac{\partial w}{\partial x} + \left( \frac{\partial w}{\partial x} \right)^2 \right) \right] dx \\ &\quad - \int_0^L \int_A p_z w dA dx \end{aligned} \tag{13}$$

where  $A_{11}$ ,  $A_{12}$ ,  $A_{22}$  and  $A_{33}$  are stiffness components and can be obtained by:

$$\{A_{11}, A_{12}, A_{22}\} = b \int_{-h/2}^{+h/2} E(z) \{1, z, z^2\} dz$$

$$A_{33} = k_s b \int_{-h/2}^{+h/2} G(z) dz \tag{14}$$

where  $k_s$ , the shear correction factor, is taken to be 5/6.

The kinetic energy ( $T$ ) of the FGP beam can be derived as follows:

$$\begin{aligned} T &= \frac{1}{2} \int_0^L \int_A \rho(z) \left( \left( \frac{\partial u}{\partial t} \right)^2 + 2z \frac{\partial u}{\partial t} \frac{\partial \theta}{\partial t} + \left( z \frac{\partial \theta}{\partial t} \right)^2 + \left( \frac{\partial w}{\partial t} \right)^2 \right) dA dx \\ &= \frac{1}{2} \int_0^L \left[ I_0 \left( \frac{\partial u}{\partial t} \right)^2 + 2I_1 \frac{\partial u}{\partial t} \frac{\partial \theta}{\partial t} + I_2 \left( \frac{\partial \theta}{\partial t} \right)^2 + I_0 \left( \frac{\partial w}{\partial t} \right)^2 \right] dx \end{aligned} \tag{15}$$

where inertia terms are:

$$\{I_0, I_1, I_2\} = b \int_{-h/2}^{+h/2} \rho(z) \{1, z, z^2\} dz \tag{16}$$

The Langrangian ( $I$ ) for the FGP beams can be written as follow:

$$\begin{aligned} I &= \frac{1}{2} \int_0^L \left[ I_0 \left( \frac{\partial u}{\partial t} \right)^2 + 2I_1 \frac{\partial u}{\partial t} \frac{\partial \theta}{\partial t} + I_2 \left( \frac{\partial \theta}{\partial t} \right)^2 + I_0 \left( \frac{\partial w}{\partial t} \right)^2 - A_{11} \left( \frac{\partial u}{\partial x} \right)^2 \right. \\ &\quad \left. - 2A_{12} \frac{\partial u}{\partial x} \frac{\partial \theta}{\partial x} - A_{22} \left( \frac{\partial \theta}{\partial x} \right)^2 - A_{33} \left( \theta^2 + 2\theta \frac{\partial w}{\partial x} + \left( \frac{\partial w}{\partial x} \right)^2 \right) \right] dx + \int_0^L q w dx \\ &\quad \times \int_A dA \end{aligned} \tag{17}$$

The relation between the internal forces and strain is;

$$N_x = A_{11} \frac{\partial u}{\partial x} + A_{12} \frac{\partial \theta}{\partial x} \tag{18}$$

$$M_x = A_{12} \frac{\partial u}{\partial x} + A_{22} \frac{\partial \theta}{\partial x} \tag{19}$$

$$Q_z = A_{33} \left( \frac{\partial w}{\partial x} + \theta \right) \tag{20}$$

By recalling the Hamilton's principle,

$$\delta \int_{t_1}^{t_2} I dt = 0 \tag{21}$$

By using the canonically conjugate momentums and their derivatives, the governing partial differential equations can be obtained in canonical form (Eqs.(22-27)). It must be noticed again that these canonical equations are obtained for the first time in this study for the dynamic response of FGP beams.

$$\frac{\partial u}{\partial x} = \frac{-A_{22}N_x + A_{12}M_x}{A_{12}^2 - A_{11}A_{22}} \tag{22}$$

$$\frac{\partial w}{\partial x} = -\theta + \frac{Q_z}{A_{33}} \tag{23}$$

$$\frac{\partial \theta}{\partial x} = \frac{A_{12}N_x - A_{11}M_x}{A_{12}^2 - A_{11}A_{22}} \tag{24}$$

$$\frac{\partial N_x}{\partial x} = I_0 \frac{\partial^2 u}{\partial t^2} + I_1 \frac{\partial^2 \theta}{\partial t^2} \tag{25}$$

$$\frac{\partial Q_z}{\partial x} = I_0 \frac{\partial^2 w}{\partial t^2} - q \tag{26}$$

$$\frac{\partial M_x}{\partial x} = I_1 \frac{\partial^2 u}{\partial t^2} + I_2 \frac{\partial^2 \theta}{\partial t^2} + Q_z \tag{27}$$

As the purpose of this study is to carry out the dynamic response of the FGP beams in the Laplace domain, the Laplace transform of the time-dependent equations is required. The transform techniques for

the first and second derivatives of a time-dependent function can be found in Spiegel [55]. The initial conditions of the motion are presumed to be zero.

$$u(x, 0) = \frac{\partial u(x, 0)}{\partial t} = w(x, 0) = \frac{\partial w(x, 0)}{\partial t} = \theta(x, 0) = \frac{\partial \theta(x, 0)}{\partial t} = 0 \quad (28)$$

Now, the inertias can be obtained in the Laplace space as follows:

$$\mathcal{L} \left[ I_0 \frac{\partial^2 u(x, t)}{\partial t^2} \right] = I_0 s^2 \bar{u} \quad (29)$$

$$\mathcal{L} \left[ I_1 \frac{\partial^2 u(x, t)}{\partial t^2} \right] = I_1 s^2 \bar{u} \quad (30)$$

$$\mathcal{L} \left[ I_0 \frac{\partial^2 w(x, t)}{\partial t^2} \right] = I_0 s^2 \bar{w} \quad (31)$$

$$\mathcal{L} \left[ I_1 \frac{\partial^2 \theta(x, t)}{\partial t^2} \right] = I_1 s^2 \bar{\theta} \quad (32)$$

$$\mathcal{L} \left[ I_2 \frac{\partial^2 \theta(x, t)}{\partial t^2} \right] = I_2 s^2 \bar{\theta} \quad (33)$$

The  $\bar{\cdot}$  demonstrates the transform form quantities in the Laplace domain and  $s$  is the Laplace parameter. Thus, the transformed set of governing ordinary differential equations is:

$$\frac{d\bar{u}}{dx} = \frac{-A_{22}\bar{N}_x + A_{12}\bar{M}_x}{A_{12}^2 - A_{11}A_{22}} \quad (34)$$

$$\frac{d\bar{w}}{dx} = -\bar{\theta} + \frac{\bar{Q}_z}{A_{33}} \quad (35)$$

$$\frac{d\bar{\theta}}{dx} = \frac{A_{12}\bar{N}_x - A_{11}\bar{M}_x}{A_{12}^2 - A_{11}A_{22}} \quad (36)$$

$$\frac{d\bar{N}_x}{dx} = I_0 s^2 \bar{u} + I_1 s^2 \bar{\theta} \quad (37)$$

$$\frac{d\bar{Q}_z}{dx} = I_0 s^2 \bar{w} - \bar{q} \quad (38)$$

$$\frac{d\bar{M}_x}{dx} = I_1 s^2 \bar{u} + I_2 s^2 \bar{\theta} + \bar{Q}_z \quad (39)$$

For the Euler-Bernoulli beam theory the second term ( $\frac{\bar{Q}_z}{A_{33}}$ ) of Eq. (35) is neglected.

### 2.3. Application of the CFM

As mentioned earlier, this solution scheme is successfully infused into other problems of solid mechanics. To examine the free and forced vibration response of the FGP beams the CFM is applied to the transformed governing ordinary differential equations (34-39). This efficient method transmutes two-point boundary values problems to initial value problems which can be solved by any available numerical methods in the literature. In this paper, we employed the fifth-order Runge–Kutta approach which is equivalent to the 7<sup>th</sup> order Taylor series solution [41]. The matrix form of Eqs. (34-39) is given below.

$$\{\bar{\mathbf{Y}}(x, s)\} = [\bar{\mathbf{w}}](x, s) \{\bar{\mathbf{Y}}(x, s)\} + \{\bar{\mathbf{F}}(x, s)\} \quad (40)$$

In the above equation  $[\bar{\mathbf{w}}](x, s)$  is the differential transition matrix,  $\{\bar{\mathbf{Y}}(x, s)\}$  and  $\{\bar{\mathbf{F}}(x, s)\}$  are state vector and load vector in the Laplace space. The boundary conditions are tabulated in Table 1.

Eq. (40) is a two-point boundary value problem which consists of a set of 6 ordinary linear differential equations. In this equation  $[\bar{\mathbf{w}}]$  a 6x6 matrix,  $\{\bar{\mathbf{Y}}(x, s)\}$  and  $\{\bar{\mathbf{F}}(x, s)\}$  vectors with 6x1 dimensions. With

the aid of the boundary conditions the general solution to Eq.(40) in the Laplace space can be derived as:

$$\{\bar{\mathbf{Y}}(x, s)\} = \sum_{m=1}^6 C_m [\bar{\mathbf{U}}^{(m)}(x, s)] + \{\bar{\mathbf{V}}(x, s)\} \quad (41)$$

The first term ( $\bar{\mathbf{U}}^{(m)}(x, s)$ ) on the right side of Eq. (41) is homogeneous solutions while the second term ( $\bar{\mathbf{V}}(x, s)$ ) is that particular solution. The linearly independent complementary solutions are obtained by giving 1 to the  $m^{\text{th}}$  whereas, zero to all the others. To obtain  $\bar{\mathbf{V}}(x, s)$  we set all initial conditions equal to zero. The integration constants,  $C_1, C_2, \dots, C_6$  are computed from the boundary conditions given in Table 1. Each problem considered in this paper has at least six boundary conditions. The theoretical framework of the CFM is available and can be found in the literature. (see [56,57]). To carry out the free vibration characteristics of the FGP beams, the Laplace parameter ( $s$ ) is replaced with “ $i\omega$ ”.  $\bar{\mathbf{V}}(x, s)$  and external loads are presumed to be zero. The matrix of the coefficients which is generated to obtain the  $C_1, C_2, \dots, C_6$  constants consist  $\omega$  values. The values of  $\omega$  which make the determinant of this matrix zero are the natural frequencies of the FGP beam.

In the case of forced vibration, the obtained results in the Laplace space are retransferred to the time domain with the aid of modified Durbin’s Inverse Laplace transform [58–60].

### 2.4. Effect of Damping

To carry out the damped forced vibration of the FGP beams, the Kelvin damping model ([61]) is utilized. The constitutive relation for the Kelvin type damping model is:

$$S_{ij} = 2G \left( e_{ij} + g \frac{de_{ij}}{dt} \right) \quad (42)$$

In the above equation  $S_{ij}$  and  $e_{ij}$  are the deviatoric components of stress and strain which can be defined in terms of stress  $\sigma_{ij}$  and strain  $\epsilon_{ij}$  as follows:

$$S_{ij} = \frac{3\sigma_{ij} - \delta_{ij}\sigma_{kk}}{3} \quad (43)$$

$$e_{ij} = \frac{3\epsilon_{ij} - \delta_{ij}\epsilon_{kk}}{3} \quad (44)$$

In Eqs (43-44) repeated indices demonstrate summation and  $\delta_{ij}$  shows Kronecker’s delta. With the aid of the correspondence principle, Laplace transform of the elasticity modulus can be derived as follows:

$$E_v(z) = E(z)(1 + gs) \quad (45)$$

where  $E_v$  is viscoelastic modulus and  $g$  is the coefficient of damping. In this case, stiffness components can be obtained by:

$$\{(A_{11})_v, (A_{12})_v, (A_{22})_v\} = b \int_{-h/2}^{+h/2} E_v(z) \{1, z, z^2\} dz$$

$$(A_{33})_v = k_s b \int_{-h/2}^{+h/2} G_v(z) dz \quad (46)$$

**Table 1**  
Boundary conditions for several restraints

Boundary conditions	atr = 0	atr = L
Clamped – Clamped (C – C)	$u = w = \theta = 0$	$u = w = \theta = 0$
Hinged - Clamped (H – C)	$u = w = M_x = 0$	$u = w = \theta = 0$
Clamped- Hinged (C – H)	$u = w = \theta = 0$	$u = w = M_x = 0$
Hinged - Hinged (H – H)	$u = w = M_x = 0$	$u = w = M_x = 0$
Clamped – Free (C – F)	$u = w = \theta = 0$	$N_x = Q_z = M_x = 0$

### 3. Results and Discussions

In this section, detailed numerical examples are carried out to examine the dynamic response of FGP beams. The influences of porosity distributions, length to height ratios, boundary conditions, shear deformation, and damping ratios are studied and highlighted. Computed results are tabulated for free vibration and illustrated in graphical forms for forced vibration response.

#### 3.1. Free vibration

In order to ascertain the accuracy of the suggested unified approach, an adequate number of validation examples have been presented. Different instances have been adduced to scrutinize the free vibration analysis of FGP beams. For the verification of the results, natural frequencies of a C-C FGP beam are carried out based on the TBT and CBT. Dimensionless natural frequencies have been computed and validated for both SMCR and MMCR material models and various slenderness ratios ( $L/h = 5, 20, 50$ ) in Table 2 and Table 3. The mechanical material properties of the FGP beam are  $\rho_1 = 7850 \text{ kg/m}^3$ ,  $E_1 = 200 \text{ GPa}$ ,  $\nu_1 = 0.33$  and  $e_0 = 0.5$ . Non-dimensional natural frequencies are obtained by Eq. (47).

$$\lambda_i = \frac{\omega_i L^2}{h} \sqrt{\frac{\rho_1}{E_1}} \quad (47)$$

As illustrated in tables 2–3, very good agreements between the results of the presented approach and those given in Ref. [36] can be clearly seen. In Ref. [36] the finite element approach was employed and 100 FGP finite elements were used in the analysis. After the verification of the suggested scheme, the natural frequencies of the FGP beam subjected to different boundary conditions are also carried out for both SMCR and MMCR material models. For this parametric study, two kinds of boundary conditions, namely C-H and C - F are considered. By employing the presented approach, non-dimensional free vibration characteristics of the C - H FGP beams based on the CBT and TBT are presented in Table 4.

Moreover, the natural frequencies for C - F boundary conditions are listed in Table 5.

As can be expected, among the considered three boundary conditions (Tables 2-5), the non-dimensional natural frequencies of the C-F beam are the smallest, and those of C-C boundary conditions are the largest. In the given tables it can be also seen that in all boundary conditions the natural frequencies obtained for the SMCR material model are greater than those obtained for MMCR. Also, FGP beams with a high ration of  $L/h$  have higher natural frequencies. In addition to all these, the natural frequencies carried out based on the TBT are generally lower than the natural frequencies of the FGP beams obtained from the EBT.

As another parametric study, the influence of the porosity coefficient on the free vibration characteristics of the FGP beams is investi-

gated for a C-C beam with a slenderness ratio of  $L/h = 5$ , and results are tabulated in Table 6. As appears in Table 6, for the smallest value of  $e_0$  ( $e_0 = 0.25$ ), natural frequencies obtained for the SMCR material model are closer to those of the MMCR material model. But, for the greatest value of  $e_0$  ( $e_0 = 0.75$ ) the difference between the free vibration characteristics obtained for these two material models becomes distinct. When the SMCR model is used, increasing the value of the porosity coefficient gives rise to an increase in the natural frequencies in FGP beams based on CBT or TBT. But, in the case of the MMCR material model, free vibration characteristics decrease with increasing the value of  $e_0$ .

As can be clearly observed in Tables (2-5) for the higher slenderness ratios the frequencies of the FGP beam based on the TBT are approximately equal those of CBT, but for lower slenderness ratios results of these two theories differ. This indicates the importance of considering the effect shear deformation in the free vibration analysis of FGP beams with lower slenderness ratios.

#### 3.2. Forced Vibration

In the current section, the forced vibration response of the FGP beams is examined with the aid of the suggested unified approach of the CFM and the Laplace transform. The obtained governing canonical equations are solved numerically for a series of Laplace parameters and the results are retransferred to the time domain through the use of an effectual inverse Laplace transfer method.

At the outset, verification of the suggested method for the forced vibration of FGP beams is performed. Since the lack of suitable data in the open literature that can be used to verify the presented procedure for the transient analysis, results are compared with those of the finite element method. In the analysis procedure with the finite element method, the commercial software package ANSYS is used. To generate the model of the FGP beams in ANSYS the cross-section of the beam is divided into 36 layers of the same thickness. A convergence study about the number of layers was given in [34]. BEAM189 is used in the analysis procedure, and the FGP beam is divided to 100 elements. Limitations, assumptions, and more detailed information about this element can be found in the user manual of the ANSYS program package. For the verification example, as seen in Fig. 2, a C - F supported FGP beam is analyzed under step dynamic load. The material model used in this example is SMCR. The material properties of the beam are  $\rho_1 = 7850 \text{ kg/m}^3$ ,  $E_1 = 200 \text{ GPa}$ ,  $\nu_1 = 0.33$  and  $e_0 = 0.5$ . In this verification case, the transient response is executed within the Timoshenko's beam theory. The geometric dimensions of the C - F beam are:  $b = 0.1 \text{ m}$ ,  $h = 0.1 \text{ m}$ , and  $L = 0.5 \text{ m}$ . The damping model is considered to be zero in this example. Results of the transient response are illustrated and compared in Figs. 3 and 4. To find more accurate results of the transient response through the use of ANSYS, selecting an adequate number of time steps is essential. Because the package uses the Newmark time integration method. In the current

**Table 2**  
Dimensionless natural frequencies of C-C FGP beams for SMCR material model

	L/h Mode	5		20		50	
		Wu [36]	Proposed method	Wu [36]	Proposed method	Wu [36]	Proposed method
CBT	$\lambda_1$	6.3393	6.3393	6.4716	6.4716	6.4792	6.4792
	$\lambda_2$	14.3794	14.3789	17.7708	17.7708	17.8492	17.8492
	$\lambda_3$	16.5216	16.5216	34.6311	34.6311	34.9578	34.9578
	$\lambda_4$	28.7624	28.7577	56.7868	56.7868	57.7105	57.7105
	$\lambda_5$	30.0004	30.0004	57.5187	57.5154	86.0649	86.0649
TBT	$\lambda_1$	5.0185	5.0184	6.3476	6.3476	6.4588	6.4588
	$\lambda_2$	11.2724	11.2715	17.0542	17.0537	17.7265	17.7262
	$\lambda_3$	14.3794	14.3789	32.3755	32.3734	34.5502	34.5490
	$\lambda_4$	18.6110	18.6071	51.5447	51.5379	56.6999	56.6964
	$\lambda_5$	26.4276	26.4166	57.5178	57.5154	83.9717	83.9634

**Table 3**  
Dimensionless natural frequencies of C-C FGP beams for MMCR material model

L/h	Mode	5		20		50	
		Wu [36]	Proposed method	Wu [36]	Proposed method	Wu [36]	Proposed method
CBT	$\lambda_1$	5.7687	5.7687	5.8807	5.8807	5.8872	5.8871
	$\lambda_2$	14.3658	14.3652	16.1529	16.1525	16.2191	16.2188
	$\lambda_3$	15.1039	15.1036	31.4917	31.4905	31.7679	31.7667
	$\lambda_4$	27.4569	27.4555	51.6680	51.6650	52.4504	52.4474
	$\lambda_5$	28.8300	28.8257	57.5170	57.5164	78.2314	78.2252
TBT	$\lambda_1$	4.7216	4.7215	5.7872	5.7872	5.8718	5.8718
	$\lambda_2$	10.7878	10.7869	15.6088	15.6083	16.1267	16.1263
	$\lambda_3$	14.3780	14.3732	29.7656	29.7636	31.4604	31.4590
	$\lambda_4$	17.9640	17.9603	47.6214	47.6149	51.6863	51.6826
	$\lambda_5$	25.6576	25.6471	57.5161	57.5138	76.6454	76.6366

**Table 4**  
Dimensionless natural frequencies of C-H FGP beams.

L/h	Mode	5		20		50	
		SMCR	MMCR	SMCR	MMCR	SMCR	MMCR
CBT	1	4.3747	3.9919	4.4602	4.0664	4.4651	4.0706
	2	13.4540	12.1909	14.4023	13.1010	14.4615	13.1530
	3	14.3789	14.4466	29.8766	27.1685	30.1447	27.4042
	4	26.0421	23.7925	50.6897	46.0667	51.4826	46.7951
	5	28.7577	28.8252	57.5154	57.4310	78.4307	71.2861
TBT	1	3.7947	3.5386	4.4125	4.0303	4.4574	4.0648
	2	10.2105	9.6538	14.0149	12.8074	14.3962	13.1038
	3	14.3789	14.3107	28.4337	26.0699	29.8890	27.2118
	4	17.8136	17.0866	46.9857	43.2422	50.7847	46.2691
	5	25.9333	25.0473	57.5154	57.3548	76.8891	70.1226

**Table 5**  
Dimensionless natural frequencies of C-F FGP beams.

L/h	Mode	5		20		50	
		SMCR	MMCR	SMCR	MMCR	SMCR	MMCR
CBT	1	1.0099	0.9181	1.0179	0.9249	1.0184	0.9253
	2	6.0333	5.5005	6.3590	5.7793	6.3788	5.7960
	3	7.1894	7.1947	17.7152	16.1059	17.8461	16.2166
	4	15.7814	14.4463	28.7577	28.7565	34.9293	31.7427
	5	21.5683	21.5896	34.4614	31.3494	57.6512	52.3973
TBT	1	0.9819	0.8969	1.0160	0.9235	1.0181	0.9251
	2	5.1638	4.8187	6.2787	5.7188	6.3656	5.7861
	3	7.1894	7.1918	17.2048	15.7192	17.7587	16.1509
	4	12.0905	11.4534	28.7577	28.7541	34.6165	31.5073
	5	19.8181	18.9926	32.7298	30.0299	56.8380	51.7842

**Table 6**  
Dimensionless natural frequencies of C-C FGP beams for different porosity coefficients.

Mode	$e_0=0.25$		$e_0=0.5$		$e_0=0.75$		
	SMCR	MMCR	SMCR	MMCR	SMCR	MMCR	
CBT	1	6.3071	6.0938	6.3393	5.7687	6.5186	5.2327
	2	15.0604	15.0584	14.3789	14.3652	13.7526	13.5322
	3	16.4828	15.9514	16.5216	15.1036	16.9090	13.9006
	4	30.0281	29.0945	28.7577	27.4555	27.5052	24.8208
	5	30.1208	30.1359	30.0004	28.8257	30.5338	27.6251
TBT	1	5.0867	4.9730	5.0184	4.7215	5.0164	4.3571
	2	11.5358	11.3494	11.2715	10.7869	11.1128	10.0356
	3	15.0604	15.0594	14.3789	14.3732	13.7526	13.7325
	4	19.1337	18.8857	18.6071	17.9603	18.2298	16.7827
	5	27.2516	26.9573	26.4166	25.6471	25.7668	24.0368

example, the number of time steps is taken to be 512 in ANSYS. While the suggested procedure solves the problem in the Laplace domain so, it is independent of the number and size of time steps.

In the solution process with the presented method, 64 Laplace parameters are used, which is equivalent to 64 steps of time in the time-space. The Laplace transform of the applied load is available in

the literature. From Figs. (3-4), very good agreement can be clearly seen for the forced vibration of FGP beams when comparing with the results of ANSYS. Thus, the accuracy of the suggested unified framework has been validated for the transient analysis. For most comprehensive information about the convergence of the forced vibration results related to the Laplace parameters and time increments see

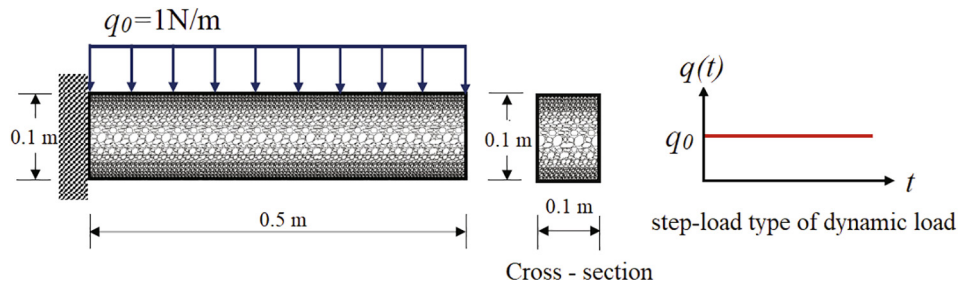


Fig. 2. The geometry of the C - F functionally graded porous (SMCR) beam and step dynamic load.

Noori et al. [62]. It can also be seen that results obtained for the coarse number of Laplace parameters fit the results of ANSYS [63] which are calculated for very fine time increments. It is obvious in Figs. 3 and 4, that in the elastic case ( $g=0$ ) the forced vibration response of FGP beams fluctuates with continuous time periods and amplitudes.

Since the accuracy of the suggested unified approach has been satisfactorily validated, now the presented method is applied to examine the transient response of the FGP beam subjected to various time-dependent loads. The material and geometric properties are the same as in the previous example.

The undamped forced vibration of a C-C supported FGP beam subject to step load ( $q_0=1\text{ kN/m}$ ) is examined for both SMCR and MMCR material models. Fig. 5 shows the maximum transverse displacement of the Euler Bernoulli beam and Fig. 6 shows the maximum vertical displacement for the Timoshenko FGP beam. In the case of TBT, the shear correction factor is assumed to be  $5/6$ .  $e_0$  is taken to be 0.5.

As might be expected, the graphical comparisons given in Figs. (5-6) shows that for both beam theories, the periods and amplitudes of vibration are greater when the FGPM is MMCR. This indicates that FGP beams made from SMCR materials have greater rigidity. Also, from Figs. (5-6) it can be seen that amplitudes of displacement are greater when influence of the shear deformation is considered (TBT).

Another parametric study is presented to examine the relationship between the transient response of the FGP beams and the coefficients of porosity,  $e_0$ . For this purpose, a C - F supported FGP beam is considered under impulsive Sine dynamic load as shown in Fig. 7. The material model of this FGP beam is assumed to be MMCR. The geometric and material properties are the same as in the previous example. Laplace transform of impulsive sine type dynamic loads is available in the literature [55].

To demonstrate the influence of the porosity coefficients on the forced vibration response of the FGP beams results are obtained and illustrated for both CBT (Fig. 8) and TBT (Fig. 9).

As clearly shown in Figs. 8 - 9, it can be seen that with increasing the coefficient of porosity of the MMCR material model, the maximum vertical displacement of the FGP beam fluctuates with larger time peri-

ods and amplitudes. In other words, when the coefficient of the MMCR increases more severe vibrations can be expected in the FGP beams based on CBT or TBT.

We now turn our attention to the damped forced vibration response of the FGP beams carried out for various damping ratios. The analogy of elastic-viscoelastic (see [61]) is employed to conduct the damped transient analysis. Stiffness components for the case of viscoelastic are given by Eq. (46).

An FGP beam with C - H supports is considered under step dynamic load ( $q_0=1\text{ kN/m}$ ) as given in Fig. 10. The material properties of the beam are  $\rho_1 = 7850\text{ kg/m}^3$ ,  $E_1 = 200\text{ GPa}$ ,  $\nu_1 = 0.33$  and  $e_0 = 0.5$ . In this case, the damped transient response is executed within the TBT. The geometric dimensions of the C - H beam are:  $b = 0.1\text{ m}$ ,  $h = 0.1\text{ m}$ , and  $L = 0.5\text{ m}$ . The material model used in this example is SMCR. The transverse deflection at the mid-span for the beam is given in Fig. 11.

Results of the viscoelastic behavior given in Fig. 11 demonstrates that the fluctuating of vibration amplitudes disappears swiftly by increasing the values of the damping ratio. The same problem is solved for CBT too and a comparison of the CBT and TBT is presented here for elastic and viscoelastic cases in Fig. 12.

As can be clearly observed in Fig. 12 for the slenderness ratio of  $L/h=5$  the amplitude and periods of the FGP beam based on the TBT are greater than those of CBT. This outlines the importance of shear deformation in the dynamic analysis of FGP beams with lower slenderness ratios.

Lastly, half rectified sine wave dynamic load function is used to examine the vibration response of the FGP beam subjected to cyclic loads. A C-C supported FGP beam (Fig. 13) made of the SMCR material model is considered. The porosity coefficient is taken to be 0.5. The natural frequency of the beam is 1617 Hz. The cyclic load with two different frequencies (1667 Hz and 833 Hz.) is applied in this example. The maximum transverse deflection of the FGP beam is obtained for both load frequencies and illustrated in Fig. (14). Laplace transform of the half rectified sine wave dynamic load function is available in the literature [55].

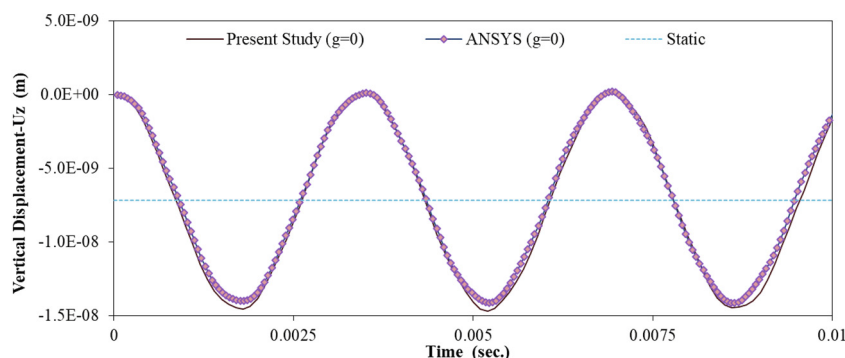


Fig. 3. Comparison of the maximum transverse deflection results of C-F FGP beam with respect to time for SMCR material model ( $e_0 = 0.5$ ).

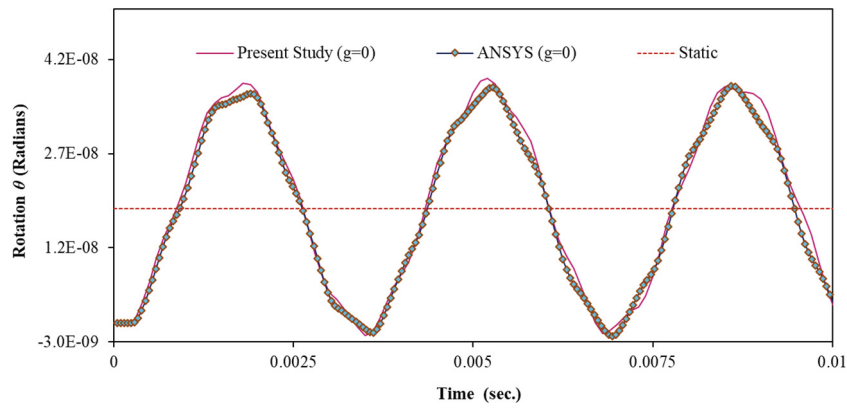


Fig. 4. Comparison of the maximum rotation results of C-F FGP beam with respect to time for SMCR material model ( $e_0 = 0.5$ ).

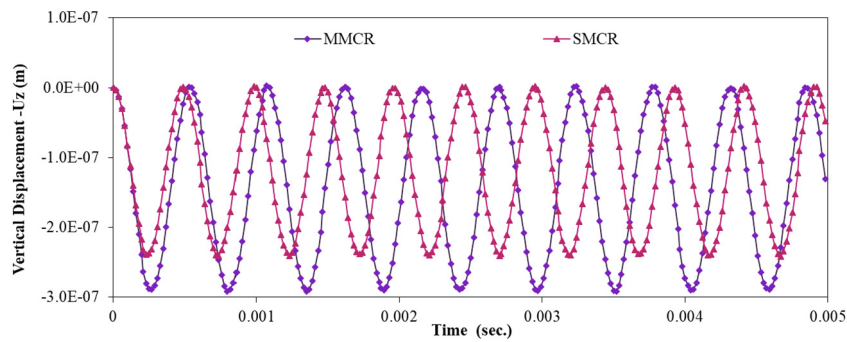


Fig. 5. Comparison of the maximum transverse deflection results of C-C FGP beam with respect to time for SMCR and MMCR material model ( $e_0 = 0.5$ ) based on the CBT.

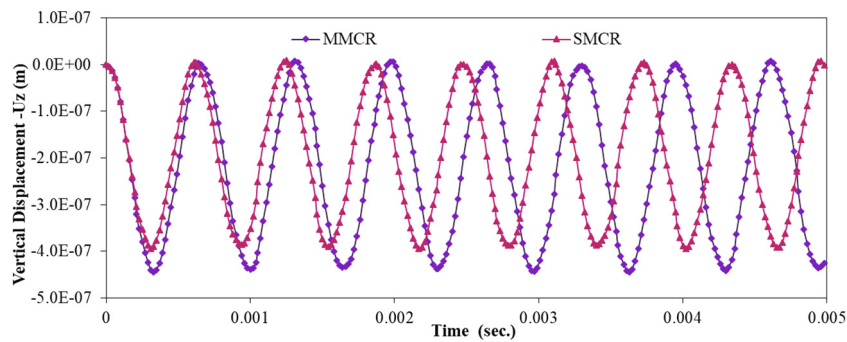


Fig. 6. Comparison of the maximum transverse deflection results of C-C FGP beam with respect to time for SMCR and MMCR material model ( $e_0 = 0.5$ ) based on the TBT.

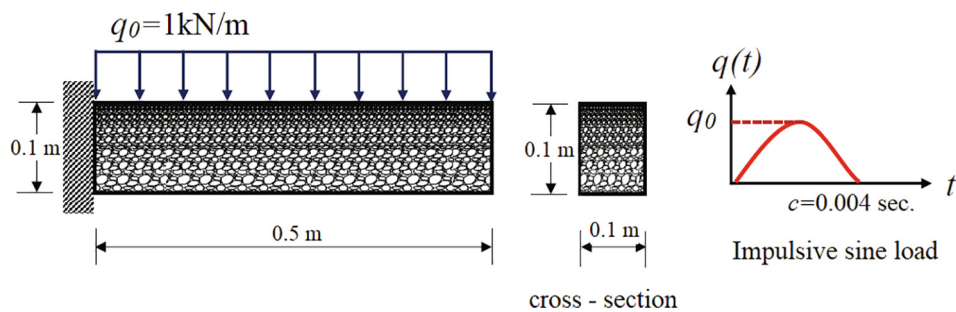


Fig. 7. The geometry of the C-F functionally graded porous (MMCR) beam and impulsive sine dynamic load.

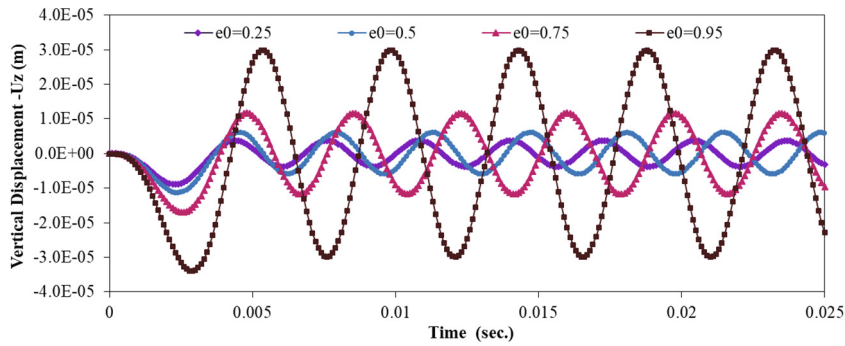


Fig. 8. Comparison of the maximum transverse deflection results of C-F FGP beam subjected to impulsive sine load with respect to time for MMCR material model based on the CBT.

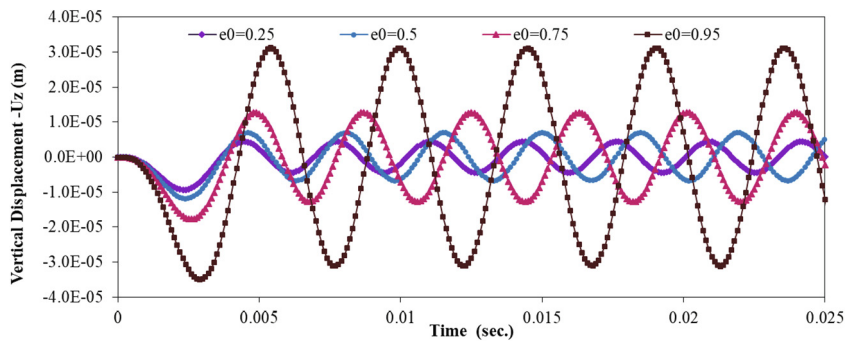


Fig. 9. Comparison of the maximum transverse deflection results of C-F FGP beam subjected to impulsive sine load with respect to time for MMCR material model based on the TBT.

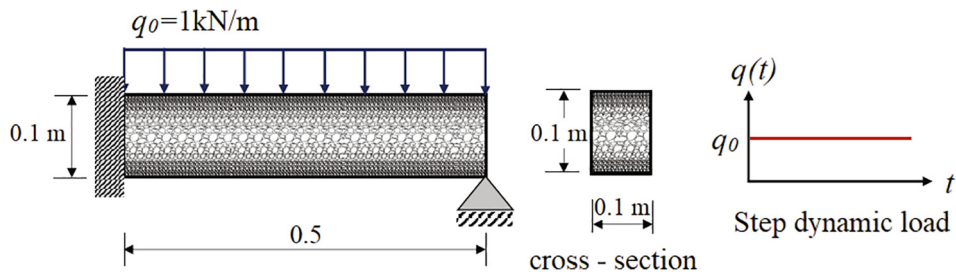


Fig. 10. The geometry of the C - H functionally graded porous (SMCR) beam and step dynamic load

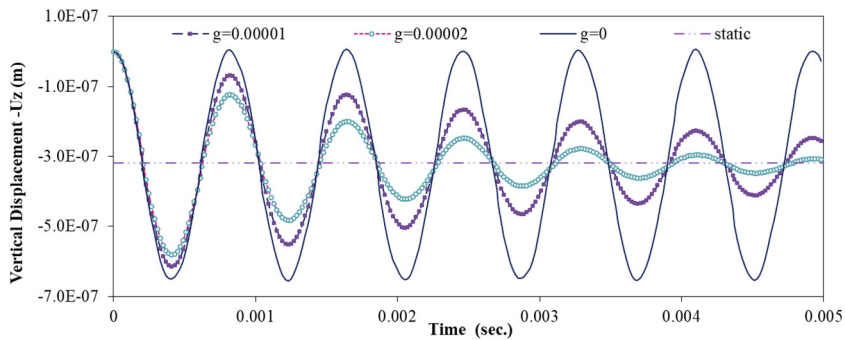


Fig. 11. Transverse deflection results of the mid-span of C - H FGP (SMCR) beam subjected to step load for various damping ratios based on the TBT.

It can be clearly observed in Fig. 14 that when the frequency of the cyclic load is 1667 Hz ( $c = 0.0003$ ) the maximum vertical displacement of the beam is also fluctuating with larger amplitudes. But when the

frequency of the applied cyclic load is 833 Hz ( $c = 0.0006$ ) the amplitudes of the vibration response get smaller. As a result, when the frequency of the applied load and the natural frequency of the FGP

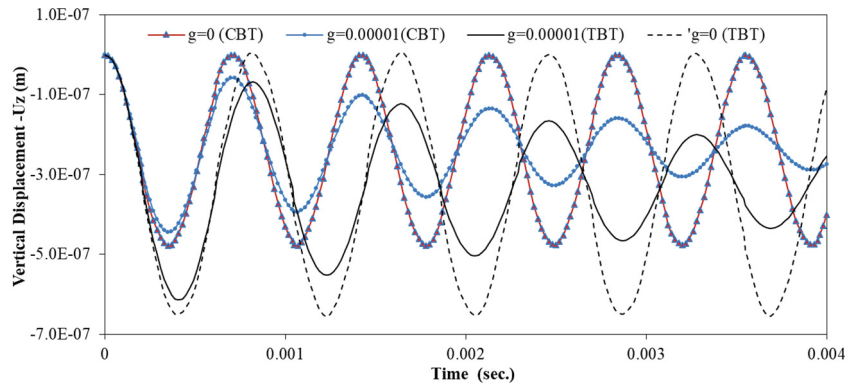


Fig. 12. Comparison of the transverse deflection results of the mid-span of C-H FGP (SMCR) beam subjected to step load for various damping ratios based on the CBT and TBT.

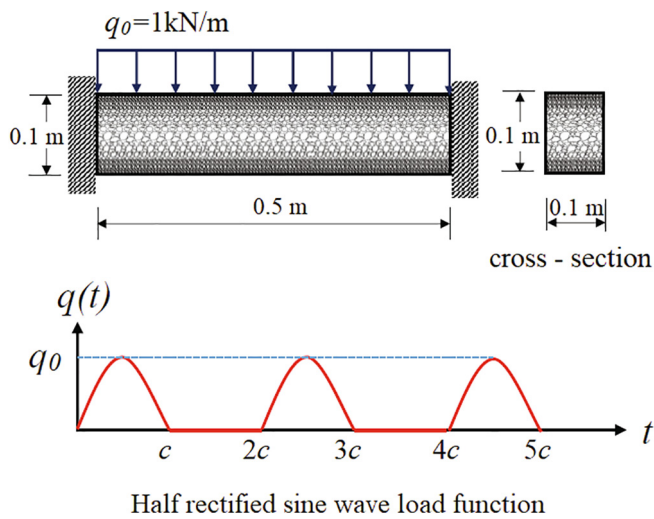


Fig. 13. The geometry of the C-C functionally graded porous (SMCR) beam and half rectified sine wave dynamic load

beams (e.g. 1617 Hz) are close to each other the beat phenomenon occurs in the structure and it would experience more violent vibration. For this reason, more severe vibration is observed when  $c = 0.0003$ .

4. Conclusion

In the current study, a unified numerical approach is presented for the free vibration and transient analysis of functionally graded porous

beams with several boundary and loading conditions. Within the presented numerical scheme, mechanical properties of the FGPMs are graded through the thickness direction of the beam. Instead of directly solving the governing differential equation, we used the canonically conjugate momentums and their derivatives to obtain the canonical form of the governing equation for the first time. Also, applying the CFM in conjunction with the Laplace transform to the elastic and viscoelastic dynamic behavior of FGP beams with symmetric and monotonic material constitutive relationships is a novel approach.

In case of forced vibration, results are obtained in the Laplace space. Then, an efficient inverse Laplace transform is implemented for retransferring the results back to the time domain. Results are presented for both the Euler-Bernoulli and the Timoshenko beam theories. The robustness, accuracy, and applicability of the presented approach have been thoroughly demonstrated by rigorously verifying results with both available literature and the finite element method. Furthermore, the influence of damping is considered in the viscoelastic dynamic analysis through the implementation Kelvin model. Predictably, analysis of damped forced vibration shows that the fluctuating of vibration amplitudes disappears swiftly by increasing the values of the damping ratio. The forced vibration of the FGP beams subjected to cyclic loads is also investigated for the first time in this study. It can be inferred that in this case, the beat phenomenon may occur which would cause more severe vibration of the structure.

The effect of the porosity factor ( $e_0$ ) on the natural frequencies of the FGP beams is examined for both SMCR and MMCR models. For smaller values of  $e_0$  natural frequencies of these two models are closer to each other, but for greater values of  $e_0$  it is vice versa. When the SMCR material model is used  $e_0$  and natural frequencies of the FGP beams are directly proportional but for the MMCR model, they are

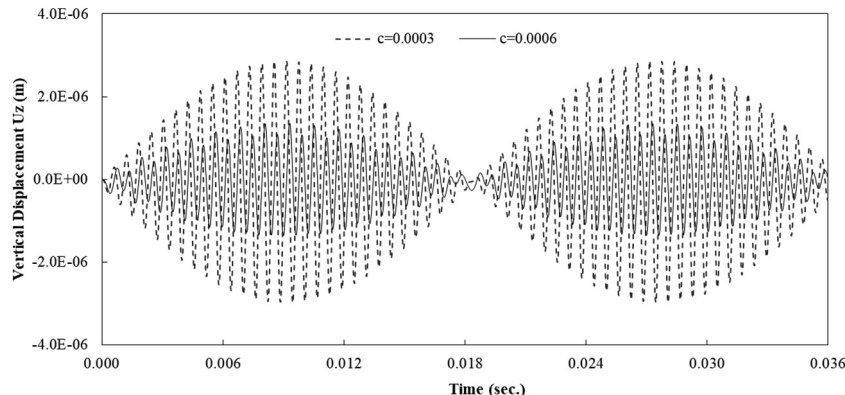


Fig. 14. Comparison of maximum vertical displacement of C - C functionally graded porous (SMCR) beam subjected to a half rectified sine cyclic dynamic load.

inversely proportional. It is stated that for lower values of slenderness ratios ( $L/h$ ) it is essential to consider the effects of shear deformation in the dynamic analysis of FGP beams. In the case of the forced vibration, it is concluded that periods and amplitudes of vibration are greater when the material of the beam is MMCR compared with SMCR. When the coefficient of porosity of the MMCR increases more severe vibrations can be expected in the FGP beams. The SMCR material offers the lowest deflection and highest natural frequency which is desired in the FGP beams in terms of stiffness.

It should be noticed that the main objective of this study is to introduce this efficient unified approach for the free and forced vibration response of the FGP beams. The presented numerical approach can be applied to any arbitrary functions of FGPBs.

## 5. Data Availability Statement

The data that support the findings of this study are available from the corresponding author, upon reasonable request.

## Declaration of Competing Interest

The authors declare that they have no known competing financial interests or personal relationships that could have appeared to influence the work reported in this paper.

## References

- [1] Shafiei N, Mirjavadi SS, MohaselAfshari B, Rabby S, Kazemi M. Vibration of two-dimensional imperfect functionally graded (2D-FG) porous nano-/micro-beams. *Computer Methods in Applied Mechanics and Engineering*. 2017;322:615–32.
- [2] Rezaei A, Saidi A. Application of Carrera Unified Formulation to study the effect of porosity on natural frequencies of thick porous–cellular plates. *Composites Part B: Engineering*. 2016;91:361–70.
- [3] Ashby MF, Evans A, Fleck NA, Gibson LJ, Hutchinson JW, Wadley HN. *Metal foams: a design guide*-Butterworth-Heinemann, Oxford, UK, ISBN 0-7506-7219-6, Published 2000, Hardback, 251 pp., \$75.00. *Materials and Design*. 2002;1(23):119.
- [4] Lefebvre LP, Banhart J, Dunand DC. Porous metals and metallic foams: current status and recent developments. *Advanced engineering materials*. 2008;10(9):775–87.
- [5] Betts C. Benefits of metal foams and developments in modelling techniques to assess their materials behaviour: a review. *Materials Science and Technology*. 2012;28(2):129–43.
- [6] Smith B, Szyniszewski S, Hajjar J, Schafer B, Arwade S. Steel foam for structures: A review of applications, manufacturing and material properties. *Journal of Constructional Steel Research*. 2012;71:1–10.
- [7] Jabbari M, Joubaneh EF, Khorshidvand A, Eslami M. Buckling analysis of porous circular plate with piezoelectric actuator layers under uniform radial compression. *International Journal of Mechanical Sciences*. 2013;70:50–6.
- [8] Li Q, Wu D, Chen X, Liu L, Yu Y, Gao W. Nonlinear vibration and dynamic buckling analyses of sandwich functionally graded porous plate with graphene platelet reinforcement resting on Winkler-Pasternak elastic foundation. *International Journal of Mechanical Sciences*. 2018;148:596–610.
- [9] Liu B, Chen H, Cao W. A novel method for tailoring elasticity distributions of functionally graded porous materials. *International Journal of Mechanical Sciences*. 2019;157:457–70.
- [10] Tian J, Zhang Z, Hua H. Free vibration analysis of rotating functionally graded double-tapered beam including porosities. *International Journal of Mechanical Sciences*. 2019;150:526–38.
- [11] Chen M, Ye T, Zhang J, Jin G, Zhang Y, Xue Y, et al. Isogeometric three-dimensional vibration of variable thickness parallelogram plates with in-plane functionally graded porous materials. *International Journal of Mechanical Sciences*. 2020;169:105304.
- [12] Bendenia N, Zidour M, Bousahla AA, Bourada F, Tounsi A, Benrahou KH, et al. Deflections, stresses and free vibration studies of FG-CNT reinforced sandwich plates resting on Pasternak elastic foundation. *Computers and Concrete*. 2020;26(3):213–26.
- [13] Menasria A, Kaci A, Bousahla AA, Bourada F, Tounsi A, Benrahou KH, Tounsi A, Bedia EAA, Mahmoud SR. A four-unknown refined plate theory for dynamic analysis of FG-sandwich plates under various boundary conditions. *Steel and Composite Structures*;2020; 36(3): 355–367.
- [14] Rabhi M, Benrahou KH, Kaci A, Houari MSA, Bourada F, Bousahla AA, et al. A new innovative 3-unknowns HSDT for buckling and free vibration of exponentially graded sandwich plates resting on elastic foundations under various boundary conditions. *Geomechanics and Engineering*. 2020;22(2):119–32.
- [15] Matouk H, Bousahla AA, Heireche H, Bourada F, Bedia EAA, Tounsi A, et al. Investigation on hygro-thermal vibration of P-FG and symmetric S-FG nanobeam using integral Timoshenko beam theory. *Advances in Nano Research*. 2020;8(4):293–305.
- [16] Chikr SC, Kaci A, Bousahla AA, Bourada F, Tounsi A, Bedia EAA, et al. A novel four-unknown integral model for buckling response of FG sandwich plates resting on elastic foundations under various boundary conditions using Galerkin's approach. *Geomechanics and Engineering*. 2020;21(5):471–87.
- [17] Refrafi S, Bousahla AA, Bouhadra A, Menasria A, Bourada F, Tounsi A, et al. Effects of hygro-thermo-mechanical conditions on the buckling of FG sandwich plates resting on elastic foundations. *Computers and Concrete*. 2020;25(4):311–25.
- [18] Rahmani MC, Kaci A, Bousahla AA, Bourada F, Tounsi A, Bedia EAA, et al. Influence of boundary conditions on the bending and free vibration behavior of FGM sandwich plates using a four-unknown refined integral plate theory. *Computers and Concrete*. 2020;25(3):225–44.
- [19] Zine A, Bousahla AA, Bourada F, Benrahou KH, Tounsi A, Bedia EAA, et al. Bending analysis of functionally graded porous plates via a refined shear deformation theory. *Computers and Concrete*. 2020;26(1):63–74.
- [20] Kaddari M, Kaci A, Bousahla AA, Tounsi A, Bourada F, Tounsi A, et al. A study on the structural behaviour of functionally graded porous plates on elastic foundation using a new quasi-3D model: Bending and free vibration analysis. *Computers and Concrete*. 2020;25(1):37–57.
- [21] Addou FY, Meradjah M, Bousahla AA, Benachour A, Bourada F, Tounsi A, et al. Influences of porosity on dynamic response of FG plates resting on Winkler/Pasternak/Kerr foundation using quasi 3D HSDT. *Computers and Concrete*. 2019;24(4):347–67.
- [22] Medani M, Benahmed A, Zidour M, Heireche H, Tounsi A, Bousahla AA, et al. Static and dynamic behavior of (FG-CNT) reinforced porous sandwich plate using energy principle. *Steel and Composite Structures*. 2019;32(5):595–610.
- [23] Berghouti H, Bedia EAA, Benkhedda A, Tounsi A. Vibration analysis of nonlocal porous nanobeams made of functionally graded material. *Advances in Nano Research*. 2019;7(5):351–64.
- [24] Yildirim S. Hydrogen elasticity solution of functionally-graded spheres, cylinders and disks. *International Journal of Hydrogen Energy*. 2020;45(41):22094–101.
- [25] Biot MA. Theory of buckling of a porous slab and its thermoelastic analogy. *ASME J Appl Mech*. 1964;31(2):194–8.
- [26] Magnucki K, Stasiewicz P. Elastic buckling of a porous beam. *Journal of Theoretical and Applied Mechanics*. 2004;42(4):859–68.
- [27] Chen D, Yang J, Kitipornchai S. Elastic buckling and static bending of shear deformable functionally graded porous beam. *Composite Structures*. 2015;133:54–61.
- [28] Jamshidi M, Arghavani J, Maboudi G. Post-buckling optimization of two-dimensional functionally graded porous beams. *International Journal of Mechanics and Materials in Design*. 2019;15(4):801–15.
- [29] Fouda N, El-Midany T, Sadoun A. Bending, buckling and vibration of a functionally graded porous beam using finite elements. *Journal of Applied and Computational Mechanics*. 2017;3(4):274–82.
- [30] Ramteke PM, Mahapatra BP, Panda SK, Sharma N. Static deflection simulation study of 2D Functionally graded porous structure. *Materials Today: Proceedings*. 2020.
- [31] Ebrahimi F, Mokhtari M. Transverse vibration analysis of rotating porous beam with functionally graded microstructure using the differential transform method. *Journal of the Brazilian Society of Mechanical Sciences and Engineering*. 2015;37(4):1435–44.
- [32] Ebrahimi F, Zia M. Large amplitude nonlinear vibration analysis of functionally graded Timoshenko beams with porosities. *Acta Astronautica*. 2015;116:117–25.
- [33] Al Rjoub YS, Hamad AG. Free vibration of functionally Euler-Bernoulli and Timoshenko graded porous beams using the transfer matrix method. *KSCIE Journal of Civil Engineering*. 2017;21(3):792–806.
- [34] Chen D, Yang J, Kitipornchai S. Free and forced vibrations of shear deformable functionally graded porous beams. *International journal of mechanical sciences*. 2016;108:14–22.
- [35] Chen D, Kitipornchai S, Yang J. Nonlinear free vibration of shear deformable sandwich beam with a functionally graded porous core. *Thin-Walled Structures*. 2016;107:39–48.
- [36] Wu D, Liu A, Huang Y, Huang Y, Pi Y, Gao W. Dynamic analysis of functionally graded porous structures through finite element analysis. *Engineering Structures*. 2018;165:287–301.
- [37] Akbaş ŞD. Forced vibration analysis of functionally graded porous deep beams. *Composite Structures*. 2018;186:293–302.
- [38] Zhao J, Wang Q, Deng X, Choe K, Xie F, Shuai C. A modified series solution for free vibration analyses of moderately thick functionally graded porous (FGP) deep curved and straight beams. *Composites Part B: Engineering*. 2019;165:155–66.
- [39] Qin B, Zhong R, Wang Q, Zhao X. A Jacobi-Ritz approach for FGP beams with arbitrary boundary conditions based on higher-order shear deformation theory. *Composite Structures*. 2020;112435.
- [40] Lei Y-L, Gao K, Wang X, Yang J. Dynamic behaviors of single-and multi-span functionally graded porous beams with flexible boundary constraints. *Applied Mathematical Modelling* 2020.
- [41] Noori AR, Aslan TA, Temel B. An efficient approach for in-plane free and forced vibrations of axially functionally graded parabolic arches with nonuniform cross section. *Composite Structures*. 2018;200:701–10.
- [42] Temel B, Noori AR. Out-of-plane vibrations of shear-deformable AFG cycloidal beams with variable cross section. *Applied Acoustics*. 2019;155:84–96.
- [43] Temel B, Noori AR. A unified solution for the vibration analysis of two-directional functionally graded axisymmetric Mindlin-Reissner plates with variable thickness. *International Journal of Mechanical Sciences*. 2020;174:105471.

- [44] Noori AR, Temel B. On the vibration analysis of laminated composite parabolic arches with variable cross-section of various ply stacking sequences. *Mechanics of Advanced Materials and Structures*. 2018;1–15.
- [45] Aslan TA, Noori AR, Temel B. Dynamic response of viscoelastic tapered cycloidal rods. *Mechanics Research Communications*. 2018;92:8–14.
- [46] Calim FF. Vibration Analysis of Functionally Graded Timoshenko Beams on Winkler-Pasternak Elastic Foundation. *Iranian Journal of Science and Technology, Transactions of. Civil Engineering*. 2019:1–20.
- [47] Calim FF. Free and forced vibration analysis of axially functionally graded Timoshenko beams on two-parameter viscoelastic foundation. *Composites Part B: Engineering*. 2016;103:98–112.
- [48] Eker M, Yarimpabuç D, Çelebi K. The Effect of the Poisson Ratio on Stresses of Heterogeneous Pressure Vessels. *European Mechanical Science*. 2018;2(2):52–9.
- [49] Yarimpabuç D, Eker M, Çelebi K. Mechanical behavior of functionally graded pressure vessels under the effect of Moisson's ratio. *European Mechanical Science*. 2018;2(2):52–9.
- [50] Temel B, Yildirim S, Tutuncu N. Elastic and viscoelastic response of heterogeneous annular structures under arbitrary transient pressure. *International Journal of Mechanical Sciences*. 2014;89:78–83.
- [51] Yildirim S, Tutuncu N. Effect of magneto-thermal loads on the rotational instability of heterogeneous rotors. *AIAA Journal*. 2019;57(5):2069–74.
- [52] Yildirim S, Tutuncu N. Radial vibration analysis of heterogeneous and non-uniform disks via complementary functions method. *The Journal of Strain Analysis for Engineering Design*. 2018;53(5):332–7.
- [53] Gibson LJ, Ashby MF. *Cellular solids: structure and properties*. Cambridge University Press; 1999.
- [54] Choi J, Lakes R. Analysis of elastic modulus of conventional foams and of re-entrant foam materials with a negative Poisson's ratio. *International Journal of Mechanical Sciences*. 1995;37(1):51–9.
- [55] Spiegel MR. *Laplace transforms: McGraw-Hill New York*; 1965.
- [56] Tutuncu N, Temel B. A novel approach to stress analysis of pressurized FGM cylinders, disks and spheres. *Composite Structures*. 2009;91(3):385–90.
- [57] Celebi K, Yarimpabuç D, Tutuncu N. Free vibration analysis of functionally graded beams using complementary functions method. *Archive of Applied Mechanics*. 2018;88(5):729–39.
- [58] Temel B. Transient analysis of viscoelastic helical rods subject to time-dependent loads. *International journal of solids and structures*. 2004;41(5–6):1605–24.
- [59] Temel B, Şahan MF. An alternative solution method for the damped response of laminated Mindlin plates. *Composites Part B: Engineering*. 2013;47:107–17.
- [60] Durbin F. Numerical inversion of Laplace transforms: an efficient improvement to Dubner and Abate's method. *The Computer Journal*. 1974;17(4):371–6.
- [61] Boley BA, Weiner JH. *Theory of thermal stresses*. Courier Corporation 2012.
- [62] Noori AR, Aslan TA, Temel B. Damped transient response of in-plane and out-of-plane loaded stepped curved rods. *Journal of the Brazilian Society of Mechanical Sciences and Engineering*. 2018;40(1):28.
- [63] ANSYS Inc Release 15.0 2013 Canonsburg, PA